

# Synthesis and characterization of nanocomposite MCM-41 ('LUS') ceramic membranes

B. Hamad<sup>1</sup>, A. Alshebani<sup>1</sup>, M. Pera-Titus<sup>1</sup>, S. Wang<sup>1</sup>, M. Torres<sup>1</sup>, B. Albela<sup>2</sup>,  
L. Bonneviot<sup>2</sup>, S. Miachon<sup>1,\*</sup> and J.-A. Dalmon<sup>1</sup>

<sup>1</sup>Institut de Recherches sur la Catalyse et l'Environnement de Lyon (IRCELYON), UMR 5256 CNRS - Université Claude Bernard Lyon 1,  
2, av. A. Einstein, 69626 Villeurbanne cedex, France

<sup>2</sup>Laboratoire de Chimie, UMR 5182, CNRS - Ecole Normale Supérieure de Lyon, 46 allée d'Italie, 69364 Lyon cedex, France

## Abstract

A new type of nanocomposite membranes, MCM-41 ('LUS')-based material networks grown into porous ceramic membrane support walls (alumina and zirconia), were prepared. Physical characterization (low-angle XRD, TPD, SEM-EDX) confirm the sole presence of the LUS mesostructure (BJH pore size  $\approx 3.2$  nm), and in a high enough amount to plug the pores of the tubular supports. Single gas hydrodynamic characterization shows that the contribution of defects (i.e. viscous flux) is negligible or comparable to reference mesoporous commercial membranes (5-nm pore size  $\gamma$ -alumina), but with a considerably enhanced permeance for gases and water, as well as a single pore size. When compared to literature results on similar organized mesoporous membranes, this work shows even greater improvements.

*Keywords:* MCM membrane, LUS, nanocomposite, pore-plugging.

## 1. Introduction

MCM silica materials were first synthesized at Mobil Oil Corporation in the early 90's [1,2] (MCM = 'Mobil Corporate Material'). This nomenclature deals with a whole class of ordered mesoporous structures belonging to the M41S family, made of silica walls organizing the porous structure in a semi-crystalline way, with uniform and tunable pore size distributions in the range 2-10 nm.

In its simplest form, the synthesis of these materials proceeds via a supramolecular templating mechanism, where a surfactant forming lyotropic liquid crystal phases serves as an organic template for the polymerization of silicate. Depending upon surfactant concentration and processing conditions, the final structure of silica exhibits hexagonal (MCM-41), cubic (MCM-48), and lamellar (MCM-50) symmetry. Other ordered mesostructured silicates, aluminosilicates and metal oxide materials (e.g., FSM, SBA, KIT, MSU, STAC, HMS [3]) have been reported as well.

MCM-41 and MCM-48 silica materials can hardly be used as adsorbents or catalysts under hydrothermal conditions because of their low structural stability ascribed to their extremely thin pore walls. The stability of MCM materials towards moisture and compression can be notably increased by silylation [4], doping with Zr [5], and vapor treatment with SnCl<sub>4</sub> before calcination [6]. Bonneviot et al. [7] have patented a new class of MCM-41 mesoporous silica termed 'LUS' (LUS = 'Laval University Silica') with higher hydrothermal stability. Three innovative points are introduced in the hydrothermal synthesis of 'LUS' silica compared to MCM-41: (1) Na<sub>2</sub>SiO<sub>3</sub> is used as Si source instead of tetraethoxysilane, (2) the counter-anion in the cationic surfactant is tosylate, which allows a different dispersion of Si-OH groups on the silica surface that leads to higher stability, and (3) the synthesis requires lower amounts of surfac-

tant, which in its turn allows better surfactant removal after the synthesis and makes the process economically advantageous.

Although sol-gel titania, silica and zirconia mesoporous membranes have been studied for long, the technological potential of templated silica films in membrane-based separation processes, heterogeneous catalysis, sensors and microelectronic devices has only been realized in recent years. A number of reviews and book chapters on the field are now available [3,8-10]. The synthesis of mesostructured silica films has been primarily accomplished at the air/water and oil/water interfaces (free standing films) (e.g., [11-13]) and on dense substrates (e.g., mica [14,15], glass [16-19], silicon wafers [14,20,21] and graphite [14,22]) either by hydrothermal treatment or through the use of solvent evaporation techniques (i.e. dip-coating, spin-coating or casting). Moreover, pulsed laser deposition [23] has also been reported to date for the fabrication of mesoporous silica films.

While all these studies are useful for developing synthetic strategies leading to the growth of mesostructured films, only a few works have attempted the synthesis of ordered silica films on porous supports. The main drawback that has been traditionally argued towards 2D hexagonal silica membranes is that, during the synthesis, the porous network tends to arrange randomly and even parallel to the support surface instead of perpendicularly, which hinders permeation. This is probably why most of the studies have concentrated on the synthesis of 3D cubic silica membranes (e.g. MCM-48) by hydrothermal treatment [24-31] and by solvent evaporation techniques [27,32-35], without spatial restrictions against permeation. To our knowledge, preferential channel orientation perpendicular to the support in silica thin film structures has only been achieved by Brossière et al. [36] (MSU-X) and by Tolbert et al. [37] (MCM-41), these latter authors using magnetic field alignment.

In this study, we have extended the nanocomposite pore plugging approach developed by some of us for palladium-

\* Corresponding author.

Sylvain.Miachon@ircelyon.univ-lyon1.fr

ceramic [38] and MFI-ceramic membranes [39-43] to the synthesis of MCM-41 'LUS' membranes with high gas and water permeation performance and with high structural stability. In this concept, the active phase is not made of a film on the top of a porous support, but rather embedded into the support pores. This structure, as opposed to more common film-like structures, presents many advantages. First, the making of a continuous defect-free area seems easier at the scale of the support pores ( $\text{nm}^2$  to  $\mu\text{m}^2$ ) than for  $\text{cm}^2$  or  $\text{m}^2$  samples. Second, individual membrane defects, if any, cannot exceed the size of the support pore. Third, the active phase is protected into the hard matrix of the support. This limits the formation of long-range stresses and provides a better mechanical resistance (in particular to scratches or vibrations), as well as a higher resistance to thermal shocks, avoiding unnecessary precautions during thermal treatments. Moreover, due to the intimate composite structure at the 100-nm scale, the thermal behavior of the nanocomposite membranes prepared so far are quite different from their film-like counterparts [41,44]. Finally, the protocols used to prepare such materials are scale-independent, making the upscale to industrial manufacturing easier to consider.

## 2. Experimental

### 2.1. Materials

The LUS precursor suspension was prepared using colloidal silica (Ludox HS-40, 40 wt.% in water, Aldrich), CTATos (cetyltrimethylammonium-p-toluene sulfonate, HPLC grade, >99% purity, Merck) as cationic surfactant, sodium hydroxide pellets (Acros, 97% purity) and ammonium acetate (Prolabo 98-100% purity). Ethanol 95% (VWR) was used as washing solution.

Before application to membrane geometry, the LUS material was synthesized on  $\alpha$ -alumina 2 to 4-mm balls (Rhône-Poulenc, type 512), with a specific surface area of  $10.5 \text{ m}^2 \cdot \text{g}^{-1}$ , porous volume of  $0.465 \text{ cm}^3 \cdot \text{g}^{-1}$  and apparent density of  $0.83 \text{ g} \cdot \text{cm}^{-3}$ .

The membranes were prepared on porous asymmetric 15-cm long tubular supports with 7 mm i.d. and 10 mm o.d. with both ends enameled, provided by Pall Exekia (Membralox T1-70). Some syntheses were also carried out on tube slices (~2.5 mm thick), for analysis purposes. Two types of commercial ceramic tubes were chosen as supports. Type 1 was made of  $\alpha$ -alumina altogether, including three layers: (i) a mechanical support made of a 1.5-mm thick, 12- $\mu\text{m}$  pore size layer, (ii) a 20- $\mu\text{m}$  thick, 0.8- $\mu\text{m}$  pore size intermediate layer, and (iii) a 14  $\mu\text{m}$  thick, 0.2- $\mu\text{m}$  pore size top layer. This support was also used in crunched form. Type 2 support was similar to the former one, but with a nm-thin layer of titania covering alumina and with a 2- $\mu\text{m}$  thick mesoporous top layer made of zirconia of 20-nm mean pore size.

### 2.2. LUS synthesis

The details on the synthesis of MCM-41 'LUS' itself as a powder can be found in ref. [45]. In this recipe, Ludox (15.5 g) was added to sodium hydroxide (2.0 g) in deionized water (50 mL), then stirred at  $15^\circ\text{C}$  until a clear solution was formed (about 24 h). A second solution of CTATos (2.5 g) in deionized water (90 mL) was stirred for 1 h at  $60^\circ\text{C}$ . The first solution was added dropwise to the second one and stirred for 2 h at  $60^\circ\text{C}$ . The resulting sol-gel was heated in an autoclave at  $130^\circ\text{C}$

for 20 h. After filtration and washing with deionized water (ca. 1000 mL), the as-synthesized was dried at  $80^\circ\text{C}$  overnight.

The protocols described below are direct adaptations of this synthesis procedure to ceramic balls and porous tubular supports.

#### *LUS synthesis in presence of alumina*

This preparation was carried out to check the compatibility of the LUS synthesis when in contact with ceramics. To this aim, 32 g of sodium hydroxide and 187 mL of Ludox were mixed in 800 mL of distilled water and left under stirring for 24 h at  $40^\circ\text{C}$ . Subsequently, 160 mL of this silicate solution were heated at  $60^\circ\text{C}$  for 1 h. At the same time, 231 mL of distilled water and 6.4 g of CTATos were stirred for 1 h at  $60^\circ\text{C}$  in a 500-mL conical flask. Then, the silicate solution was poured, drop by drop, into the surfactant solution at reduced stirring, and left at  $60^\circ\text{C}$  under stirring for 2 h until obtaining a clear solution of silica.

This precursor solution (125 mL) was then poured down into an autoclave reactor, together with 4 g of alumina balls or crushed membrane, and submitted to hydrothermal synthesis at  $130^\circ\text{C}$  for 20 h. The solid was then filtered, washed with water, dried at  $80^\circ\text{C}$  overnight. In order to separate the powder LUS from the LUS agglomerated with alumina, the solid was then sieved. Later on, it was subjected to removal of the surfactant.

#### *LUS membrane synthesis*

This preparation was carried out using a pore-plugging approach similar to the one described for zeolite membrane synthesis in previous papers [38], but using the protocol described above. However, to avoid air trapping in the pores, the precursor solution was introduced into the tubular support matrix by the action of vacuum. The total volume of precursor solution was 35 mL per tube, leaving 15 mL of free gas volume in the autoclave. The tube slices were added on top of the tube in the autoclave.

#### *Surfactant removal*

The removal of surfactant from the mesopores of the material was carried out by washing. This was achieved (either for ball or tubular forms) using 600 mL of 1%wt. ammonium acetate ethanol solution at  $60^\circ\text{C}$  for 30 min, before filtering and rinsing with ethanol. This procedure was repeated before drying at  $80^\circ\text{C}$  in air. A calcination step was added in some cases for better removal efficiency, as the material can withstand this type of treatment. It was carried out under  $360 \text{ NmL} \cdot \text{min}^{-1}$  air stream at  $550^\circ\text{C}$  for 5 h, using  $3^\circ\text{C} \cdot \text{min}^{-1}$  ramps.

### 2.3. Characterization techniques

#### *Characterization of LUS material*

The structure of the LUS material obtained after synthesis was characterized by low angle X-ray diffraction (LAXRD) (Cu  $K\alpha_1$  radiation on a Bruker D5005,  $\lambda = 1.54184 \text{ \AA}$ ) in the range  $1-10^\circ$  with a  $0.02^\circ$  step width and an acquisition time of 10 s per step.

The amount of LUS material synthesized on the supports, the amount of surfactant removed by calcination, was obtained from TGA/DTG analyses (Netzsch STA 409 PC) of the extracted and calcined LUS powders, as well as for the powders from the crushed membrane material, in the temperature range  $25-1000^\circ\text{C}$  using a heating rate of  $10^\circ\text{C} \cdot \text{min}^{-1}$  under air flow.

The morphology of the synthesized LUS material was inspected by scanning electron microscopy (SEM) (FEI XL30 FEG+, under low gas pressure, with no sample metallization), operating at 15 kV, while the Si concentration profile along the membrane thickness was characterized by energy dispersive X-

ray analysis (EDX) using a 1- $\mu\text{m}$  microprobe (Edax Phoenix) with SETW polymer window parallel to the membrane surface. Knowing the density of the host and LUS materials, the Si profile allows obtaining an average pore-plugging ratio in the different porous layers of the support.

The textural properties of the LUS material were obtained from  $\text{N}_2$  adsorption isotherms at 77 K on the calcined alumina balls and crushed membrane slices using a Micromeritics ASAP 2020 sorptometer. BET surface areas were determined from recorded adsorption data in the range  $0.30 \leq P/P^0 \leq 0.50$  [-], while the pore volume and pore size distribution was determined by the Barrett-Joyner-Halenda (BJH) method, [46] suited to the characterization of cylindrical pores.

#### Permeation performance of the as-synthesized membranes

The synthesized membranes and supports, after drying in an oven at  $180^\circ\text{C}$ , were submitted to both bubble point and  $\text{N}_2$  permeance testing using a home-made permeameter. In both cases, the membranes were mounted in dead-end configuration using flat gaskets pressed onto the enameled tube ending cross-section, the membrane being immersed in an ethanol bath (bubble point) or open to the atmosphere ( $\text{N}_2$  permeance). Both the pressure and the flow rate were measured at the inlet of the tube. For bubble pressure measurements, the membranes were soaked in the ethanol bath for at least 1 h before testing.

More accurate single gas permeance experiments were carried out in two other test benches using a membrane module fitted with graphite and Viton<sup>®</sup> o-rings and pressure control on both sides of the membrane. This allowed *in-situ* treatment at  $180^\circ\text{C}$  for 2 hours to desorb water from the LUS material. Hydrogen, helium, nitrogen and argon permeances were measured in dead-end configuration as a function of the average pressure (from 101 to 707 kPa) under a constant 0.7 to 1.5-kPa transmembrane pressure to evaluate the presence of defects or cracks in the LUS material. For comparison, some measurements were also carried out on a reference commercial  $\gamma$ -alumina asymmetric membrane (5 nm-mean pore size).

The evolution of single gas permeance with the average pressure provides relevant information dealing with the density of inter-crystalline defects in the LUS structure. In general terms, single gas permeance across this type of membrane occurs either by Knudsen diffusion or viscous flow. In the case of mesoporous membranes, gas permeation is mainly governed by Knudsen diffusion. Nevertheless, if large defects are present (e.g., pinholes and cracks), viscous flow can contribute significantly to mass transfer. For weakly or non-interacting gases, the permeance within a porous membrane can be expressed as:

$$\Pi = \frac{\varepsilon}{\tau \ell} \left( \frac{d_p}{3} \sqrt{\frac{8}{\pi MRT}} + \frac{d_p^2 P_m}{32 \mu_G RT} \right) = \alpha + \beta P_m$$

with:

- $d_p$ : mean pore size [m]
- $\ell$ : membrane equivalent thickness [m]
- $M$ : Molecular weight of the gas [ $\text{kg m}^{-3}$ ]
- $P_m$ : mean pressure [Pa]
- $R$ : ideal gas constant [ $8.314 \text{ Pa m}^3 \text{ mol}^{-1} \text{ K}^{-1}$ ]
- $T$ : temperature [K]
- $\varepsilon$ : porosity [-]
- $\mu_G$ : gas viscosity [ $\text{kg m}^{-1} \text{ s}^{-1}$ ]
- $\Pi$ : gas permeance [ $\text{mol m}^{-2} \text{ s}^{-1} \text{ Pa}^{-1}$ ]
- $\tau$ : tortuosity [-]

The first term in the right-hand side of this expression accounts for Knudsen diffusion, while the second one is ascribed to viscous flow. In this way, the representation of permeance

against the average pressure results in a straight line where the intercept value ( $\alpha$ ) represents the Knudsen flux and the slope ( $\beta$ ) corresponds to the viscous contribution. When applying this equation to gas permeance within a mesoporous membrane, such as those synthesized in this study, high slopes or  $\beta$  values will be indicative of a high density of large intercrystalline defects in the membrane. Let us underline that, here, the large average pressure range allows for a precise evaluation of the presence of defects, if any.

Steady-state water permeance was also measured in dead-end mode, both in the vacuum-wetted fresh supports and LUS-modified membranes, as a function of back-pressure (0-202 kPa), applied constantly by means of a  $\text{N}_2$ -pressurized autoclave.

## 3. Results

### 3.1 Material characterization

#### Low-angle XRD

In order to assess for the influence of the presence of the substrate in the final mesostructure of the LUS material, some preliminary experiments were carried out in which LUS was prepared as a powder and on alumina balls and crushed alumina tube slices. The low angle XRD patterns obtained for the samples prepared on all supports show typical peaks of LUS material, exclusively to any other crystalline structure. As an example, Fig. 1 shows the low-angle XRD patterns of the LUS powder material prepared in contact with crushed alumina tube pieces. These patterns reveal the desired 2D hexagonal structure of MCM-41 type, irrespective of the method chosen for surfactant removal (i.e. washing or calcination). Note that the peaks become more intense and definite after surfactant removal due to an increase of contrast after emptying the channel of the siliceous structure.

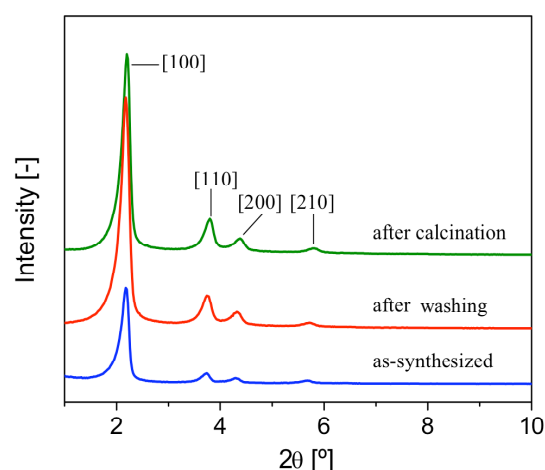


Fig. 1. Low-angle XRD patterns of LUS powder material as-synthesized in contact with crushed porous alumina, and after removal of the surfactant by washing and calcination.

Moreover, all the peaks remain present after washing and calcination, staying approximately at the same position. In fact, there is an expansion of about 2% after washing and a contraction of the same amplitude after calcination. As a result, the final calcined LUS shows the same XRD position as the initial LUS containing the surfactant. The structure does not change and undergoes a slight 'breath', bringing the material to about the same lattice parameter in the calcined form. This is one of

the specificities of LUS compared to MCM-41, which usually contracts upon calcination. Note that this LUS was prepared in the presence of alumina beads to assess for the robustness of the synthesis in presence of alumina, and that the beads were removed from the powder analysed here.

To assess for the structure of the LUS material when prepared in membrane form, with very low amounts of LUS material, some XRD analyses were performed on membrane crushed pieces. Fig. 2 shows the XRD patterns obtained before and after calcination in the narrow range 1.5-4.5°, with higher accumulation time, to improve the accuracy of the measurements. In this case, the d(100) distance contracts ca. 8% after calcination from an initial value of 4.1 nm.

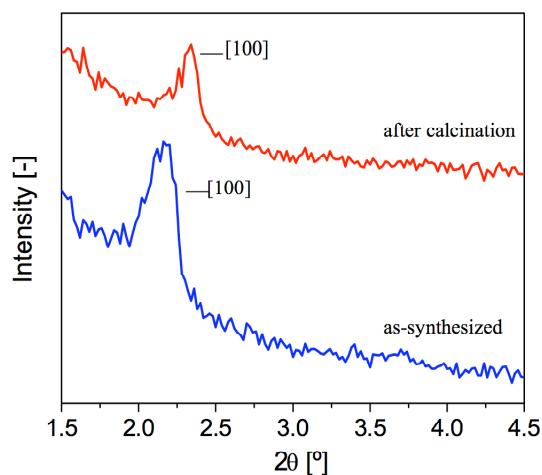


Fig. 2. Low-angle XRD patterns of LUS material as-synthesized on crushed porous alumina tubes, and after removal of the surfactant by washing and calcination.

### Weight gain and TGA/DTG analyses

Fig. 3 shows the TGA and DTG weight curves for LUS material synthesized as a powder and on porous alumina slices, before and after calcination. In all cases, one observes a first peak corresponding to water desorption at about 120°C, and, in the case of uncalcined samples, two additional peaks at: (i) ~250-330°C, where most of the surfactant decomposition occurs and (ii) ~400-600°C, ascribed to silanol group condensation.

The quantification of the LUS material deposited on each substrate was calculated after the result obtained on the LUS powder. The weight loss at 1000°C on as-made LUS was 49%, meaning that the remaining 51% were pure LUS. The calcined sample weight loss was limited to 6%, mainly due to water desorption, as can be seen on the DTG curve. Therefore, the surfactant removal and silanol condensation are responsible for 43% of the weight loss of any uncalcined sample.

Table 1 lists the results obtained from gravimetric analysis of the different substrates used in this study after LUS synthesis. In the case of full-length tubular supports, weight uptake could be accurately determined using a balance (for a total increase of about 40 mg). However, in the case of alumina balls and alumina tube slices, the extremely low weight uptake values could only be accurately obtained from TGA analysis. The amount of LUS was then inferred from the total weight loss at 1000°C with the proportion of 49/51.

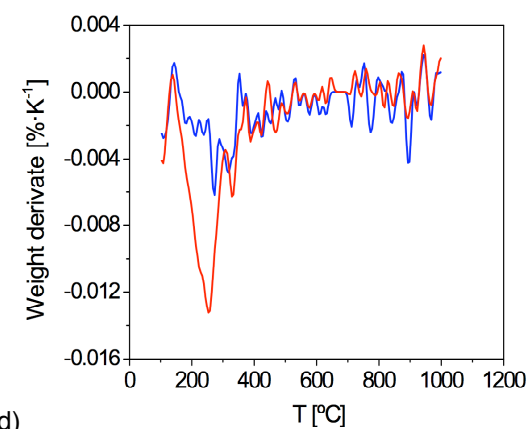
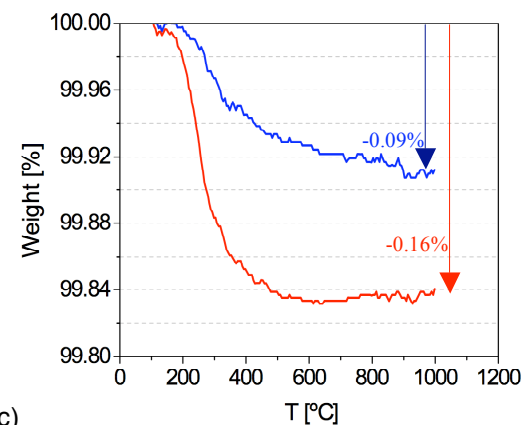
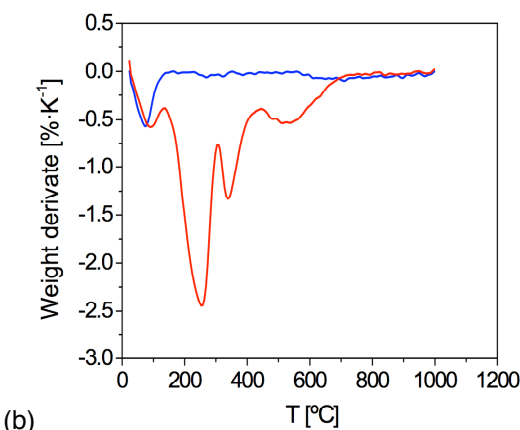
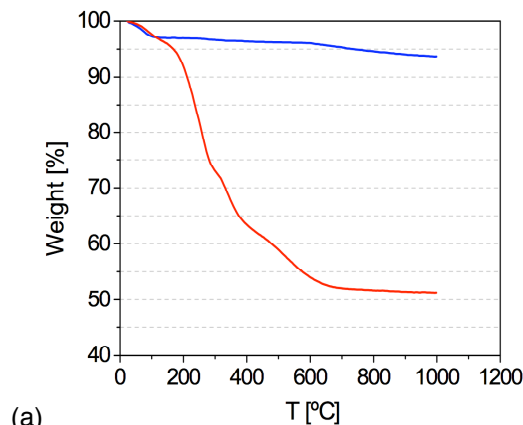


Fig. 3. TGA/DTG weight curves of LUS material as pure powder (upper plots (a) and (b)) and prepared on slices of porous alumina (lower curves (c) and (d)), before removal of the surfactant (red curves) and after calcination (blue curves).

170 Table 1

Typical weight loss at 1000°C before (fresh sample) and after calcination and the computed LUS mass [wt.%] of LUS material on the different substrates used in this study. Under the dashed line, direct weight uptake of the membranes.

Support	Weight loss		Computed LUS mass	Mass uptake after synthesis
	Before	After		
Alumina balls (DTG)	1.5%	0.3%	1.5%	
Tube slice (DTG)	0.16%	0.09%	0.16%	
-----				
Full-length tube type 1 (from direct weight measurement):				0.23%
Full-length tube type 2 (from direct weight measurement):				0.23%

### Nitrogen adsorption

Table 2 shows the BET specific surface areas obtained in the N<sub>2</sub> adsorption experiments after calcination. The first column indicates the very high specific surface area of LUS material (1159 m<sup>2</sup>·g<sup>-1</sup>). As a consequence, synthesis of this material on low-surface area material, such as alumina balls or alumina Type 1 tubes, with specific surface ~0.03 m<sup>2</sup>·g<sup>-1</sup>, results in a remarkable increase of this parameter after calcination. This allows quantifying the LUS material present on each substrate, as shown in Table 2.

The pore size distribution of the synthesized LUS (not shown) is very narrow and centered at 3.2 nm, according to the BJH model. A pore wall thickness of less than 1 nm can then be estimated when comparing this pore size to the interplanar 100 distance computed from the XRD patterns on the same material.

Table 2

BET specific surface area of the LUS material on itself, and of two substrates before and after LUS synthesis [m<sup>2</sup>·g<sup>-1</sup>]. In parentheses, estimated corresponding values of LUS material on each substrate.

LUS [m <sup>2</sup> ·g <sup>-1</sup> ]	Al <sub>2</sub> O <sub>3</sub> balls [m <sup>2</sup> ·g <sup>-1</sup> ]		Type 1 tube slices [m <sup>2</sup> ·g <sup>-1</sup> ]	
	before	after	before	after
1159 ± 3	10.5	13.4 ± 0.1 (1.16 wt.%)	0.03	1.26 ± 0.01 (0.106 wt.%)

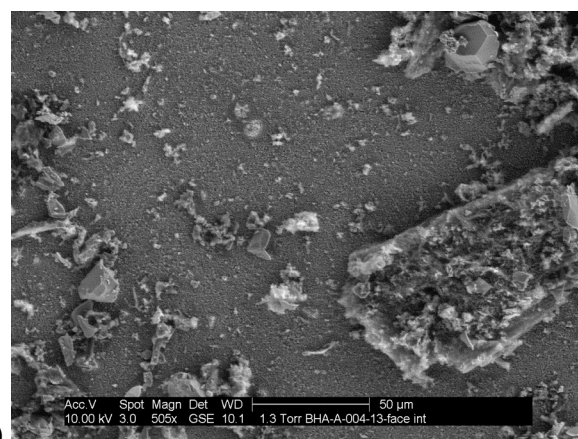
### Electron microscopy

A complete electron microscopy study was carried out, mainly on a broken alumina tubular supported LUS modified membrane and on its corresponding tube slices supported samples. The goal of these measurements was to locate silicon-based material on top and within the tube porous wall, and to quantify its proportion related to the ceramic support. Fig. 4 displays typical micrographs of a LUS – alumina membrane (cross-section and surface).

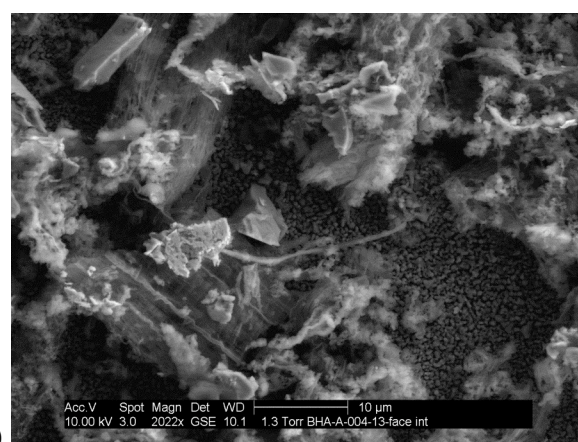
On the cross-section views (Fig. 4 bottom micrographs), large semi-crystals containing mainly silica (as can be also seen by EDX microprobe analysis) appear all over the observed thickness. These structures form dendrite-like extension on top of the support top-layer, made of fibres of ca. 200-nm diameter, as is usually structured LUS material. Surface micrographs of these extensions (Fig. 4 top micrographs) clearly show that no continuous film layer is formed on top of the support.

To obtain further information on the average concentration of silica as a function of depth into the support, EDX window analysis was performed. Fig. 5 shows such a typical procedure, as well as the resulting graph of atomic Si/Al ratios as a function of depth. Surface EDX analysis (from the membrane top-layer side) provided similar values of atomic silica/alumina

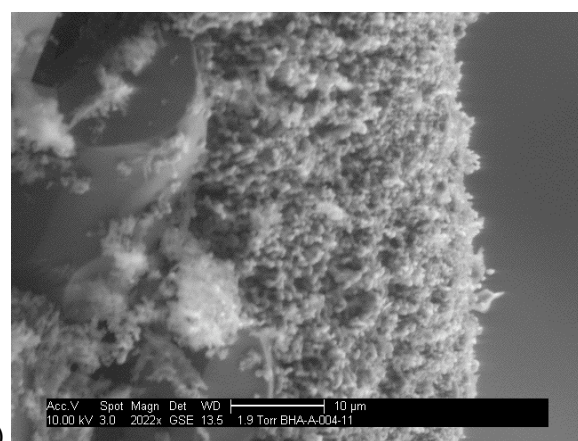
ratios (about 0.06) in the region where no conglomerate was present (such as the centre of Fig. 5 top view).



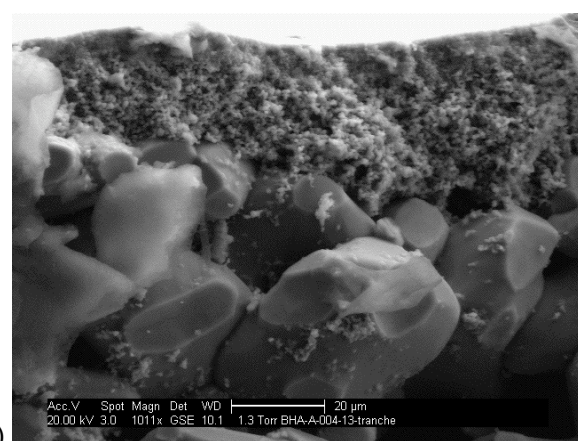
(a)



(b)

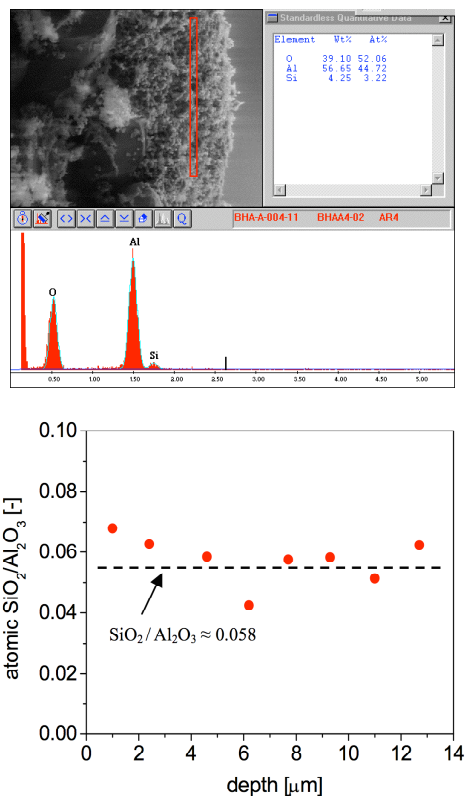


(c)



440 (d)

Fig. 4. SEM top-views (a) & (b), and cross-section views (c) & (d) of a LUS – alumina nanocomposite membrane (after calcination, type 1).



145 Fig. 5. EDX analysis using a series of 2 x 35 μm windows of a LUS – alumina composite membrane (type 1 support). Top: typical analysis, bottom: distribution of the silica/alumina ratio over the top-layer thickness.

### 3.2. Transport characterization

150 After preparation of the LUS – ceramic material in dispersed form, membrane preparation was carried out. This section presents bubble tests, as well as water and gas permeance results.

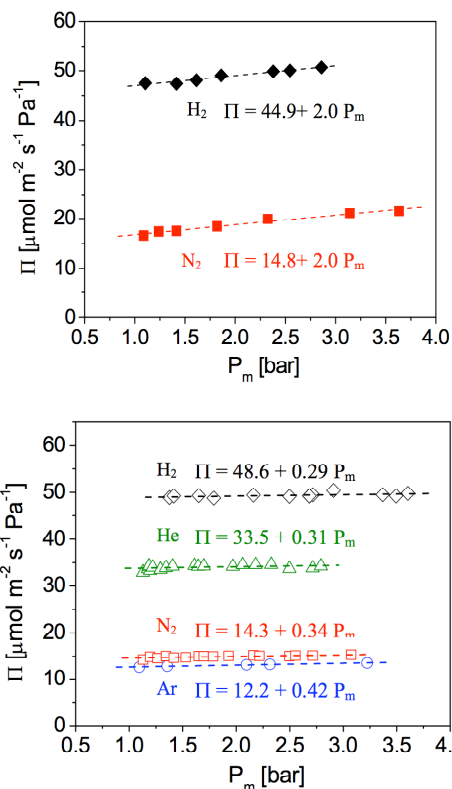
#### Single gas permeance tests

155 A first series of tests were carried out using single gas permeation experiments for hydrogen, helium, nitrogen and argon at room temperature after in-situ thermal treatment at 180°C for washed and calcined membranes of Type 1 and Type 2 before any further treatment.

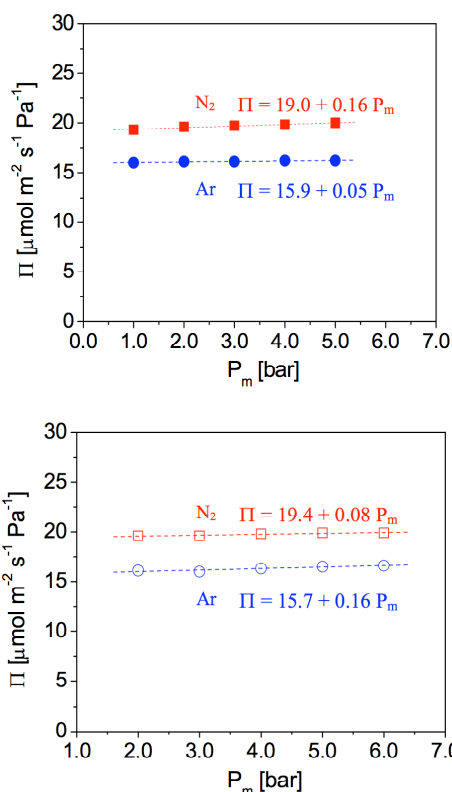
160 Fig. 6 shows the evolution of the single gas permeance as a function of average pressure for the supports, as well as for the nanocomposite LUS membranes. As expected, the permeance of the LUS membranes is lower than that of the corresponding support (-70 to -90%). Moreover, the linear trends that describe the evolution of the gas permeance with the average pressure are much steeper in the case of the support (not shown) than for LUS membranes. This result reflects a lower viscous contribution for the latter membranes.

170 The same samples were then subjected to post-treatment with ethanol and water at room temperature (24 hours each) and tested in a similar way. Fig. 7 shows the linear trends of the single gas permeance with the average pressure in this case. As can be seen, the N<sub>2</sub> and Ar single gas permeance are ca. 30% higher.

175 Table 3 summarizes the results of the linear fittings, expressed in viscous flow contribution at 1 bar average pressure for the plots displayed in Fig. 7, as well as for their supports and for a reference commercial 5-nm-mean-pore-size γ-alumina membrane. Regardless of the support used in the synthesis of LUS membranes, the viscous contribution to mass transfer is very low (<1%).



485 Fig. 6. Single gas permeance as a function of the average pressure for Type 1 (closed symbols, top) and Type 2 (open symbols, bottom) membranes before post-treatment with ethanol. The temperature and the trans-membrane pressure were kept, respectively at 21-25°C and at 0.7 kPa in all experiments



490

495 Fig. 7. Single gas permeance as a function of the average pressure for Type 1 (closed symbols, top) and Type 2 (open symbols, bottom) membranes after post-treatment with ethanol. The temperature and the trans-membrane pressure were kept, respectively at 21-25°C and at 1.5 kPa in all experiments.

Table 3.

Permeance ( $\Pi$ ,  $\mu\text{mol}\cdot\text{m}^{-2}\cdot\text{s}^{-1}\cdot\text{Pa}^{-1}$ ) and viscous flow (i.e. defect) contribution to the flow at 1 bar average pressure for Type 1 and Type 2 supports before and after LUS synthesis with 1-day post-treatment with ethanol and water after calcination, and a reference commercial membrane (5-nm  $\gamma$ -alumina), as calculated from linear fitting parameters of pure gas permeance vs. average pressure plots.

	Fresh support		Synthesis + post-treatment	
	$\Pi$ [ $\mu\text{mol}\cdot\text{m}^{-2}\cdot\text{s}^{-1}\cdot\text{Pa}^{-1}$ ]	%visc.	$\Pi$ [ $\mu\text{mol}\cdot\text{m}^{-2}\cdot\text{s}^{-1}\cdot\text{Pa}^{-1}$ ]	%visc.
<i>Type 1</i>				
N <sub>2</sub>	-	-	19.3 ± 0.1	0.8% ± 0.2%
Ar	115 ± 1	25% ± 1%	16.0 ± 0.1	0.3% ± 0.2%
<i>Type 2</i>				
N <sub>2</sub>	136 ± 1	7% ± 1%	19.5 ± 0.1	0.4% ± 0.2%
Ar	47 ± 1	12% ± 1%	15.9 ± 0.1	1.0% ± 0.3%
<i>5-nm <math>\gamma</math>-alumina commercial membrane:</i>				
H <sub>2</sub>	16.5 ± 0.1	0.3% ± 0.3%		
Ar	4.4 ± 0.1	0.7% ± 1.0%		

Fig. 8 shows the variation of single gas permeance (hydrogen) as a function of temperature (expressed as inverse square root). The correlation with linearity can be related to the dominant Knudsen transport mechanism.

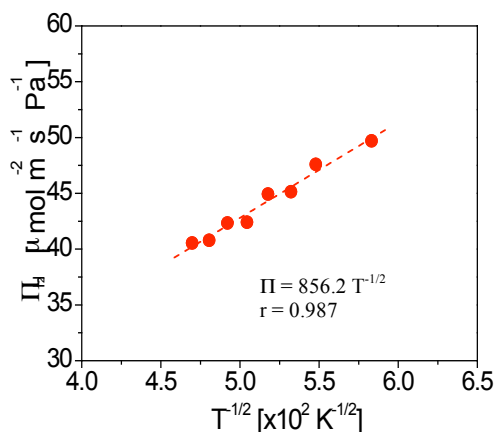


Fig. 8. H<sub>2</sub> permeance as a function of temperature. for a Type 2 membrane before post-treatment. Average pressure 303 kPa, transmembrane 0.7 kPa.

#### Ethanol bubble tests and water permeance tests

The first bubble trans-membrane pressures are provided in Table 4, together with water permeance values on both types of tubular supports and on the resulting membranes after LUS synthesis. These values are compared to commercial  $\gamma$ -alumina 5-nm top-layer tubes measured on the same bench (FBP of 150 kPa, and water permeance  $\approx 11 \mu\text{mol m}^{-2} \text{s}^{-1} \text{Pa}^{-1}$ ), corresponding to the value given by the provider (70 L/m/h/bar).

## 4. Discussion

### 4.1. Pore contraction in LUS in the presence of alumina

In pure LUS material, the removal of the surfactant reduces the value of compressive forces on the surface, which leads to the expansion of the network and therefore to a displacement to

lower angles in the XRD patterns after calcination. However, this behavior is not observed when the LUS is synthesized as a powder in the presence of alumina. In this case, a pore contraction  $\sim 2\%$  is observed, as calculated from peak displacement to higher angles in the XRD patterns shown in Fig. 1. This contraction might be ascribed to a reduction of the rigidity of the pore walls in the LUS structure due to partial incorporation of Al into its composition.

Table 4

First bubble pressure (relative to the atmosphere, FBP) in ethanol, and water permeance of the two types of support before and after LUS synthesis

	Type 1 tubes		Type 2 tubes	
	Before	after	before	after
FBP [kPa]	80-170	220	100	130
Water permeance [ $\mu\text{mol m}^{-2} \text{s}^{-1} \text{Pa}^{-1}$ ]	136 ± 20	40 ± 4	70 ± 10	19 ± 2

560

This pore contraction is even more remarkable when the LUS is synthesized in a porous alumina substrate (8% contraction vs. 2% in LUS powder). This could be consistent with a higher level of aluminium incorporation into the LUS domains leading to a larger contraction effect under calcination. Another explanation might be simply physical in nature, i.e., merely due to the size effect of the LUS domains themselves that are confined into the alumina pores. This domain size should be in the order of the pore size of alumina (0.2  $\mu\text{m}$ ). Nano-domains are known to be affected by very strong compressive forces coming from surface tension that could be released in this case after surfactant removal, thus enhancing pore contraction.

### 4.2. Amount of LUS and surfactant removal

The weight uptake directly measured on the tubular membranes (0.23%) is higher than what was inferred from the total weight loss at 1000°C (TWL1000) in TGA analysis on the tube slices (0.16%). This difference can be found in two other sets of data.

First, the total weight loss of a calcined slice of tube (Fig. 3, third graph) is much higher than it should be. As a matter of fact, the calcined powder LUS TWL1000 is 6%, about an 8<sup>th</sup> of the TWL1000 of the as-made sample. Therefore, in the case of the calcined membrane, the TWL1000 should be close to 0.02%, instead of a measured 0.09%. This excess of 0.07% happens to be the same than that one measured by direct gravimetry (0.23%-0.16%), and can therefore be affected to surfactant remaining in the structure after calcination at 550°C. Moreover, the fact that this 0.07% weight loss is due to remaining surfactant can be deduced when looking at the temperature of the removal: the derivative curve (fig. 3, 4<sup>th</sup> plot) suggests a main peak at about 240°C.

Second, the BET surface area of the tubular membrane implies an MCM uptake 0.106%wt of the powder (Table 2), instead of an expected 0.16%wt (as from TGA). The lacking surface area (a third of expected) can be attributed to remaining surfactant hindering access of nitrogen to a third of the LUS surface area, corresponding to a third of the initial surfactant mass, i.e.  $\approx 0.06\%$ . This value again matches fairly well the difference underlined in the first paragraph of this section.

Therefore, the amount of pure LUS (without surfactant) synthesised in the membrane is about 0.16%, that is  $\sim 28 \text{ mg}$ , a third

of which can be thought to be still occupied by surfactant after removal. This was observed before post-treatment. After post-treatment in ethanol and water, the gas permeance slightly increased (compare Figs. 6 and 7). This could be explained by a further amount of surfactant removed from the LUS membrane pores. As a matter of fact, it can be thought that if the initial calcination at 550°C could be sufficient on dispersed powder, this is not the case when the LUS material is embedded within the porous network of the ceramic supports. An additional diffusion hindrance in the case of the nanocomposite membrane, due to a longer outward diffusion path for the surfactant species, could originate this difference.

#### 4.3. Pore-plugging in porous supports

On the SEM micrographs (Fig. 4) no film can be seen on the top of the support. This is confirmed by a local EDX analysis of the top view, on the areas where the structure is similar to that observed on the bear support. In these zones, the silica / alumina ratio is 6%, similar to the value observed in the depth of the membrane (Fig. 5). As can be seen, the silicon/alumina ratio is fairly constant along the thickness of the two external layers, at the above value. Taking into account the relative density of the host ceramic (~3.7 g.cm<sup>-3</sup>) and the LUS (~0.9 g.cm<sup>-3</sup>), as well as the porosity of the ceramic support (25-30%) such a ratio indicates an important proportion of pores filled by MCM material, in agreement with a nanocomposite membrane structure.

#### 4.4. Membrane quality

For both membrane types, the viscous contribution is strongly reduced from the corresponding values of the fresh support after LUS synthesis due to a reduction of the  $\beta$  values (see Table 3). Considering the accuracy of this measurement, the viscous contribution could even be lower in reality, that is to say almost negligible. This result confirms the presence of a very low amount of large intercrystalline defects.

The increase of gas permeance between the first and the second sets of measurements might be attributed to additional removal of surfactant still blocking mesopores in the LUS network after calcination (the lower slope in Fig. 7 than in Fig. 6 for N<sub>2</sub> and Ar was attributed to a better sealing).

Knudsen control in mass transfer within these membranes can be also visualized through calculation of  $\alpha(\text{H}_2) / \alpha(\text{Ar})$ ,  $\alpha(\text{He}) / \alpha(\text{Ar})$  and  $\alpha(\text{N}_2) / \alpha(\text{Ar})$  ratios. From the trends depicted in Fig. 7, these ratios are, for Type 2 membrane, 4.0, 2.7 and 1.2, respectively, which are very close to the corresponding ideal Knudsen selectivities 4.47, 3.16 and 1.19. Moreover, in good keeping with the aforementioned calculations, H<sub>2</sub> permeance evolves linearly with the square root of temperature, as shown in Fig. 8.

Although the LUS membranes show high quality in terms of low viscous contribution ascribed to a low density of large defects, a very small number of defects in the LUS structure cannot be totally ruled out. The presence of large defects can be experimentally assessed from the bubble tests performed on both the fresh supports and on the supports further modified with LUS material. As can be seen in Table 4, the first bubble pressure does not change much after LUS synthesis. This result suggests that these very few large defects are not filled up by the LUS material. However, the number is so reduced that it does not translate into significant viscous contribution to the total mass transfer in gas permeation. In any case, it has to be noted that the quality of the LUS membranes prepared in this

work are of a very similar defect quality than a commercial sol-gel  $\gamma$ -alumina membrane with larger, 5-nm, pores (Table 3).

The viscous contribution measurement method could not completely rule out mesoporous defects larger than MCM pores but small enough to support no viscous flow. However, the nitrogen adsorption pore size distribution (not shown) of a crushed membrane piece was very sharp around the 3.2-nm value. Therefore, a significant presence of other size crossing pores can be excluded.

#### 4.5. Membrane performance in water permeance

As expected, the water permeance is reduced from the corresponding values obtained for the supports due to pore plugging by the LUS material (see Table 4). The water permeance of the synthesized membranes is up to 40  $\mu\text{mol}\cdot\text{m}^{-2}\cdot\text{s}^{-1}\cdot\text{Pa}^{-1}$  (Type 1), which is significantly higher than the values observed through  $\gamma$ -alumina membranes and those published for film-like mesoporous silica (MCM, SBA and MSU), and for MCM-filled polymeric membranes (see Table 5 for comparison). Note that, when compared to its Ar permeance, the water permeance of LUS-Type 2 appears low. This is likely due to the higher mass transfer resistance of the 20 nm support.

Table 5

Summary of water permeance data ( $\Pi_w$ ) at room temperature through mesoporous membranes of this work and the literature

Material	Mean pore size [nm]	$\Pi_w$ [ $\mu\text{mol}\cdot\text{m}^{-2}\cdot\text{s}^{-1}\cdot\text{Pa}^{-1}$ ]	Ref.
$\gamma$ -alumina (commercial)	5.0	11	This study
LUS-Type 1	3.2	40	“
LUS-Type 2	3.2	19	“
-----			
MCM-48	0.9-1.2	0.30	[47]
	2.3-2.6	0.45	[48]
	2.8-3.4	0.76	[49]
	1.8	1.1-4.5	[50]*
SBA-15	7.5	1.3	[51]
MSU-X	2.0-3.0	1.1	[52]
MCM-41-filled sodium alginate	-	<0.1	[53]*

\* Values obtained by pervaporation

## 5. Conclusions

Nanocomposite MCM-41 (‘LUS’) – alumina mesoporous membranes with a negligible amount of defects and high water permeability have been successfully synthesized using the pore-plugging approach. To our best knowledge, this is a first time that an MCM-41 based membrane is reported in the literature.

Owing to the embedment of the MCM material into the support pores, the nanocomposite architecture may originate the following advantages:

- As the size of MCM self supported fibre is close to (type 1 membrane) or larger than (type 2) the support pores, one can expect that inside the matrix, a LUS grain fills up the pore, and develops a close contact with the pore wall, as was observed on nanocomposite MFI membranes [44]. Therefore, here as well, grain boundary effects, that could limit the selectivity, can be less important than in film-like structures.

- The growth of the bidimensional LUS structure should be facilitated towards the axis of the support pores, thus resulting in a general orientation of the LUS pores in the direction of transmembrane transfer.

Further studies will precise the intimate structure of the nanocomposite, using in particular advanced microscopy techniques. Application development is in progress towards modifying the pore surface for hydrophobic or selective adsorption processes.

The results presented in this work open stimulating research lines for the synthesis new membranes with large potential applications.

## Acknowledgements

The Libyan embassy in Paris is greatly acknowledged for A. Alshebani's grant. M. Pera-Titus grant is part of the European Marie-Curie Program (project # 041297). F. Beauchene carried out the electron microscopy analysis.

## References

- [1] C.T. Kresge, M.E. Leonowicz, W.J. Roth, J.C. Vartuli, J.S. Beck, *Nature* 359 (1992) 710.
- [2] J.S. Beck, J.C. Vartuli, W.J. Roth, M.E. Leonowicz, C.T. Kresge, K.D. Schmitt, C.T.-W. Chu, D.H. Olson, E.W. Sheppard, S.B. McCullen, J.B. Higgins, J.L. Schlenker, *J. Am. Chem. Soc.* 114 (1992) 10834.
- [3] V.V. Gulians, M.A. Carreon, Y.S. Lin, *J. Membr. Sci.* 235 (2004) 53.
- [4] K.A. Koyano, T. Tatsumi, Y. Tanaka, S. Nakata, *J. Phys. Chem. B* 101 (1997) 9436.
- [5] N. Nishiyama, H. Saputra, D.H. Park, Y. Egashira, K. Ueyama, *J. Membr. Sci.* 218 (2003) 165.
- [6] N. Nishiyama, M. Yamaguchi, Y. Nishiyama, Y. Egashira, K. Ueyama, *J. Non-Cryst. Solids* 351 (2005) 3218.
- [7] L. Bonneviot, M. Morin, A. Badiei, Patent WO 01/55031 A1, 2001.
- [8] L.G.A. van de Water, Th. Maschmeyer, *Topics in Catalysis* 29 (2004) 67.
- [9] K.J. Edler, S.J. Roser, *Int. Reviews in Physical Chemistry* 20 (2001) 387.
- [10] A. Ayral, A. Julbe, Ch. Guizard, *Ceramic membrane processing: new approaches in design and applications*, in: *Chemical Processing of Ceramics*, 2<sup>nd</sup> Edition, Elsevier, Amsterdam, pp. 652-654.
- [11] C. Liu, J. Wang, B. Li, *J. Non-Cryst. Solids* 351 (2005) 409.
- [12] H. Yang, N. Coombs, I. Sokolov, G.A. Ozin, *Nature* 381 (1996) 589.
- [13] S. Schacht, Q. Huo, I.G. Voigt-Martin, G.D. Stucky, F. Schuth, *Science* 273 (1996) 768.
- [14] I.A. Aksay, M. Trau, S. Manne, I. Honma, N. Yao, L. Zhou, P. Fenter, P.M. Eisenberg, S.M. Gruner, *Science* 273 (1996) 892.
- [15] H. Yang, A. Kuperman, N. Coombs, S. Mamiche-Afara, G.A. Ozin, *Nature* 379 (1996) 703.
- [16] N. Shimura, M. Ogawa, *J. Colloid Interf. Sci.* 303 (2006) 250.
- [17] M. Ogawa, H. Ishikawa, T. Kikuchi, *J. Mater. Chem.* 8 (1998) 1783.
- [18] M. Ogawa, M. Masukawa, *Micropor. Mesopor. Mater.* 38 (2000) 35.
- [19] Z. Hua, J. Shi, L., W. Zhang, *J. Non-Cryst. Solids* 292 (2001) 177.
- [20] D. Zhao, P. Yang, N. Melosh, J. Feng, B.F. Chmelka, G.D. Stucky, *Adv. Mater.* 10 (1998) 1380.
- [21] Y.F. Lu, R. Ganguli, C.A. Drewien, M.T. Anderson, C.J. Brinker, W.L. Gong, Y.X. Guo, H. Soyez, B. Dunn, M.H. Huang, J.I. Zink, *Nature* 389 (1997) 364.
- [22] H. Yang, N. Coombs, I. Sokolov, G.A. Ozin, *J. Mater. Chem.* 7 (1997) 1285.
- [23] K.J. Bakus Jr., A.S. Scott, M.E. Gimon-Kinsel, J.H. Blanco, *Micropor. Mesopor. Mater.* 38 (2000) 97.
- [24] C. Liu, J. Wang, Z. Rong, *J. Membr. Sci.* 287 (2007) 6.
- [25] O. de la Iglesia, M. Pedernera, R. Mallada, Z. Lin, J. Rocha, J. Coronas, J. Santamaria, *J. Membr. Sci.* 280 (2006) 867.
- [26] P. Kumar, J. Ida, S. Kim, V.V. Gulians, J.Y.S. Lin, *J. Membr. Sci.* 279 (2006) 539.
- [27] L. Huang, S. Kawi, K. Hidajat, S.C. Ng, *Mater.* 82 (2005) 87.
- [28] N. Nishiyama, D.H. Park, Y. Egashira, K. Ueyama, *Sep. Purif. Tech.* 32 (2003) 127.
- [29] N. Nishiyama, D.H. Park, A. Koide, Y. Egashira, K. Ueyama, *J. Membr. Sci.* 182 (2001) 235.
- [30] D.H. Park, N. Nishiyama, Y. Egashira, K. Ueyama, *Ind. Eng. Chem. Res.* 40 (2001) 6105.
- [31] N. Nishiyama, A. Koide, Y. Egashira, K. Ueyama, *Chem. Commun.* (1998) 2147.
- [32] L. Huang, S. Kawi, K. Hidajat, S.C. Ng, *Micropor. Mesopor. Mater.* 88 (2006) 254.
- [33] K. Nakagawa, M. Matsuyama, T. Maki, M. Teramoto, N. Kubota, *Sep. Purif. Tech.* 44 (2005) 145.
- [34] B.A. McCool, N. Hill, J. DiCarlo, W.J. DeSisto, *J. Membr. Sci.* 218 (2003) 55.
- [35] Y.-S. Kim, S.-M. Yang, *Adv. Mater.* 14 (2002) 1078.
- [36] C. Brossière, M.U. Martines, A. Larbot, E. Prouzet, prepared with non-connecting parallel pores, *J. Membr. Sci.* 251 (2005) 17.
- [37] S.H. Tolbert, A. Firouzzi, G.D. Stucky, B.F. Chmelka, *Science* 278 (1997) 264.
- [38] S. Miachon, A. Mazuy, J.-A. Dalmon, *Stud. Surf. Sci. Catal.* 130 (2000) 2693.
- [39] S. Miachon, E. Landrison, M. Aouine, Y. Sun, I. Kumakiri, Y. Li, O. Pachtová Prokopová, N. Guilhaume, A. Giroir-Fendler, H. Mozzanega, J.-A. Dalmon, *Nanocomposite J. Membr. Sci.* 281 (2006) 228.
- [40] L. van Dyk, L. Lorenzen, S. Miachon, J.-A. Dalmon, *Catal. Today* 104 (2005) 274.
- [41] P. Ciavarella, H. Moueddeb, S. Miachon, K. Fiaty, J.-A. Dalmon, *Catal. Today* 56 (2000) 253.
- [42] A. Giroir-Fendler, J. Peureux, H. Mozzanega, J.-A. Dalmon, *Stud. Surf. Sci. Catal.* 101A (1996) 127.
- [43] D. Uzio, J. Peureux, A. Giroir-Fendler, J.-A. Dalmon, J.D.F. Ramsay, *Stud. Surf. Sci. Catal.* 87 (1994) 411.
- [44] S. Miachon, I. Kumakiri, P. Ciavarella, L. van Dyk, K. Fiaty, Y. Schuurman, J.-A. Dalmon, *J. Membr. Sci.* 298 (2007) 71.
- [45] S. Abry, B. Albel, L. Bonneviot, *C.R. Chimie* 8 (2005) 741.
- [46] E.P. Barret, L.G. Joyner, P.P. Halenda, *J. Am. Chem. Soc.* 73 (1951) 373.
- [47] S.R. Chowdhury, A.M. Peters, D.H.A. Blank, J.E. ten Elsof, *J. Membr. Sci.* 279 (2006) 276.
- [48] R. Schmuhl, S.R. Chowdhury, J.E. ten Elsof, A. van den Berg, D.H.A. Blank, *J. Sol-Gel Sci. Tech.* 31 (2004) 249.

- 325 [49] S.R. Chowdhury, R. Schmuhl, K. Keizer, J.E. ten Elsof, D.H.A. Blank, *J. Membr. Sci.* 225 (2003) 177.
- [50] D.H. Park, N. Nishiyama, Y. Egashira, K. Ueyama, *Micropor. Mesopor. Mater.* 66 (2003) 69.
- [51] T. Kang, S. Oh, H. Kim, J. Yi, *Langmuir* 21 (2005) 5859.
- 330 [52] C. Brossière, M.A.U. Martines, P.J. Kooyman, T.R. de Kruijff, A. Larbot, E. Prouzet, *Chem. Mater.* 15 (2003) 460.
- [53] S.D. Bhat, B.V.K. Naidu, G.V. Shanbhag, S.B. Halligudi, M. Sairam, T.M. Aminabhavi, *Sep. Purif. Tech.* 49 (2006) 56.